Hindawi
Journal of Applied Mathematics
Volume 2022, Article ID 7568695, 11 pages
https://doi.org/10.1155/2022/7568695

Research Article

Hydrodynamic Boundary Layer Flow of Chemically Reactive Fluid over Exponentially Stretching Vertical Surface with Transverse Magnetic Field in Unsteady Porous Medium

M. Sulemana,[1] **I. Y. Seini**,[2] **and O. D. Makinde**[3]

[1]*Department of Mathematics, University for Development Studies, Nyankpala Campus, P. O. Box 1350, Tamale, Ghana*
[2]*School of Engineering, University for Development Studies, Nyankpala Campus, P. O. Box 1350, Tamale, Ghana*
[3]*Faculty of Military Science, Stellenbosch University, Private Bag X2, Saldanha 7395, South Africa*

Correspondence should be addressed to M. Sulemana; musahsulemana@uds.edu.gh

Received 13 February 2022; Revised 30 March 2022; Accepted 23 May 2022; Published 23 June 2022

Academic Editor: Anum Shafiq

This article addresses the hydrodynamic boundary layer flow of a chemically reactive fluid over an exponentially stretching vertical surface with transverse magnetic field in an unsteady porous medium. The flow problem is modelled as time depended dimensional partial differential equations which are transformed to dimensionless equations and solved by means of approximate analytic method. The results are illustrated graphically and numerically and compared with previously published results which shown a good agreement. Physically increasing Eckert number of a fluid amplifies the kinetic energy of the fluid, and as a novelty, the Eckert number under the influence of chemically reactive magnetic field is effective in controlling the kinematics of hydrodynamic boundary layer flow in porous medium. Interestingly, whilst the Eckert number amplifies the thermal boundary layer thickness and velocity as well as the concentration of the fluid, the presence of the magnetic field and the strength of the chemical reaction have a retarding effect on the flow. Also, the chemical reaction parameter and permeability of porous medium are effective in reducing skin friction in chemically reactive magnetic porous medium and are relevant in practice because reduced skin friction enhances the efficiency of a system. The results of the current study are useful in solar energy collector systems and materials processing.

1. Introduction

Heat and mass transfer are greatly influenced by the hydrodynamic boundary layer of the flow. Recently, researchers have developed much interest in the study of hydrodynamic boundary layer flow in porous medium under the effects of a magnetic field because of the possible applications in engineering systems and industrial. In industrial and engineering operations, heat as well as mass transfer are crucial processes. They take place simultaneously in hot rolling, paper manufacturing, wire drawing, plastic manufacturing, glass fiber manufacturing, rubber sheet manufacturing, and the cooling of hot metal plates, among others. To accomplish equal cooling of the product, these processes sometime require stretching materials in a fluid media. The quality of the finished product is determined by the rate at which it is stretched and cooled. The mechanical qualities of the final product are depended on the thermal conductivity, which varies linearly with temperature [1].

Sakiadis [2] was the first to investigate fluid flow with a constant velocity on a continuous surface. Crane [3] expanded Sakiadis' work to include flows on an elastic sheet. Using a shooting approach, Chiam [4] investigated viscous fluid flow across a porous stretched sheet with varying thermal conductivity and found that the thermal conductivity amplifies the fluid temperature. Misra et al. [5] enhanced this by looking at the heat flow problem with both stretching surface temperature and stretching heat flux. Chen [6] investigated heat transfer on a stretched plate in a fluid flow, which was broadened by Ishak and colleagues [7] to incorporate magnetic field intensity on the flow. As a result of higher skin friction coefficient experienced in the flow, they

discovered that the magnetic field strength tends to decay the flow. Dandpat and Chakraborthy [8] examined the effects of properties of variable fluid flow on a stretching surface and realized that the variable viscosity of the fluid decreased the velocity profiles.

In the last decade, many researchers have worked on the subject of magnetohydrodynamics (MHD) as well as flow in porous media. In fact, the usefulness of flow in porous medium under the effects of magnetic field is enormous. It is applied to investigate the underground water in agricultural engineering, filtration, and purification process in chemical engineering to investigate the movement of water, oil, or natural gas in reservoirs in the petroleum engineering, among others. Due to the applications mentioned above, several researchers studied MHD flow in a porous medium with varied configurations, which the present study also seeks to contribute. Hsiao [9, 10] studied magnetohydrodynamics convection flow of viscoelastic fluid using finite difference method and magnetohydrodynamics stagnation flow of viscoelastic fluid subject viscous dissipation effect. He concluded that the strength of the magnetic field adversely affects the heat transfer rate. Furthermore, Nadeem et al. [11] analyzed MHD fluid properties over a linearly stretching sheet embedded in porous medium using the Runge-Kutta method and concluded that the magnetic field retards the flow. Similarly, Seini and Makinde [12] examined MHD fluid flow on stretching sheet with radiation and chemical reaction effects. A nonlinear velocity term attributed to the magnetic field presence was included in the energy equation, and results revealed that the heat transfer rate decreased with the magnetic field and the radiation parameter. Ali et al. [13] extended Seini and Makinde work to include heat transfer in inclined stretching sheet with magnetic field. Similarly, Sahoo et al. [14] analyzed the MHD viscoelastic flow on a stretching plate and found that fluids with larger Prandtl numbers adversely affect the temperature due to low thermal diffusivity. Ahmed et al. [15] studied numerical/analytical solutions for MHD flow in porous medium past oscillating vertical sheet and realized that the shear stress and fluid velocity depressed as a result of increment in permeability parameter whilst the velocity and the temperature profiles decreased due to an increased in conduction-radiation parameter. Krishna el al. [16] extended Ahmed et al. [15] study to an unsteady flow on an infinite oscillating porous vertical sheet and observed the same trends. Sulemana et al. [17] applied Laplace transform method to study unsteady boundary layer flow on a vertical surface subject to heat source and magnetic field in porous medium. Also, Sulemana et al. [18] extended their study in [17] to examine unsteady convective flow on a vertical surface subject to porous medium with Newtonian heating. They concluded in both studies that the heat absorption parameter decays the temperature. Recently, Sulemana and Seini [19] studied time-dependent hydromagnetic flow on a vertical plate in porous medium and concluded that as time passed, skin friction coefficient reduced. Hussain et al. [20] studied MHD viscoinelastic fluid flow on stretching plate using the law of Fourier heat conduction and observed that the movement of fluid is defied by strength of the magnetic field. Khan et al. [21] analyzed non-Newtonian flow on a stretching/shrinking permeable surface using HAM. It was established that increased values of radiation parameter enhanced the temperature whilst the temperature fell for the rising Prandtl number. Chemical reaction effect on MHD dissipative nanofluid on slippering stretching surface embedded in porous medium is investigated by Yousef et al. [22]. They observed that in the absence of magnetic field, the nanofluid experiences a faster velocity. Saeed et al. [23] studied MHD Casson flow on stretching surface in porous medium using HAM. The influence of chemical reaction is also investigated in this study. They noticed a reduction in mass fluid diffusivity due to increasing values of chemical reaction. Homogeneous-heterogeneous reactions on three-dimensional, MHD flow on exponentially stretching/shrinking sheet is studied by Algehyne et al. [24]. In this investigation, the effects of chemical reaction and magnetic field are also considered. It was observed that the velocity along the x-direction and the y-direction is reduced by the stretching ratio parameter. Similarly, Rasheed et al. [25] investigated the effects of chemical reaction and hall current on unsteady MHD flow past a vertical surface employing ND-solve method in Mathematica and observed that the temperature of the fluid developed with increased in Schmidt number, Eckert number, and radiation parameter but diminished with the Prandtl number.

To authors' best knowledge, hydrodynamic boundary layer flow of a chemically reactive fluid over an exponentially stretching vertical surface with transverse magnetic field in an unsteady porous medium is not documented. The present study attempts to investigate the problem using approximate analytic method. In the current study, the works of Ahmed et al. [15] and Krishna *et al.* [16] are extended to include the influence of chemically reactive in a magnetic porous medium under unsteady conditions over nonoscillating stretching vertical surface. The chemical reaction species is introduced in the flow because of its practical applications in diffusional operations in many engineering systems. The results obtained by the approximate analytic method used in the current study indicate that chemically reactive magnetic field can be used to influence the flow field.

2. Mathematical Formulation of the Problem

Consider a magnetohydrodynamic flow on stretching vertical surface in a chemically unsteady porous reactive medium. The flow assumptions are as follows:

(i) The flow is unsteady

(ii) The stretching plate is taken along the x^*-axis direction

(iii) The y^*-axis is at right angle to the surface

(iv) A magnetic field of uniform strength, B_0 is applied transversely to the plate

(v) The Reynolds number is assumed to be too small; hence, the induced magnetic field is negligible

(vi) Also, viscous dissipation is further assumed to be too small hence neglected

(vii) The ambient fluid temperature and the plate temperature are T^*_∞ and $T^*_w(x)$, respectively

(viii) At first, the fluid and the stretching plate are at the same temperature T^*_∞ with concentration level C^*_∞ at all points

(ix) For time $t^* > 0$, the surface is moving continuously with an exponential velocity $u = U_w(x) = U_0(1 - e^{at})$ in the positive x^*-direction and the temperature of the stretching plate is linearly with t^*

(x) The concentration levels closer to the plate are raised to C^*_w

(xi) The physical properties of the fluid like thermal conductivity and viscosity and shall be assumed constant

(xii) The plate is infinitely along the x^*-direction; hence, all the physical parameters are functions of y^* and t^* only

(xiii) Gray fluid, nonscattering but absorbing/emitting radiation is used in the analysis

Figure 1 shows the physical fluid flow system.

By the assumptions above and extending the works of Ahmed et al. [15] and Krishna et al. [16] with nonoscillating but stretching vertical surface under the influence of chemically reactive in a magnetic porous medium, the equations of the boundary layer are as follows:

$$\frac{\partial u^*}{\partial x^*} + \frac{\partial v^*}{dy^*} = 0, \tag{1}$$

$$\frac{\partial u^*}{\partial t^*} - V\frac{\partial u^*}{dy^*} = \upsilon\frac{\partial^2 u^*}{\partial y^{*2}} + g\beta_T(T^* - T^*_\infty) + g\beta_C(C^* - C^*_\infty) - \frac{\sigma B_0^2}{\rho}u^* - \frac{\upsilon}{k^*}u^*, \tag{2}$$

$$\frac{\partial T^*}{\partial t^*} - V\frac{\partial T^*}{dy^*} = \alpha\frac{\partial^2 T^*}{\partial y^{*2}} + \frac{\upsilon}{c_p}\left(\frac{\partial u^*}{\partial y^*}\right)^2 + \left(\frac{\upsilon}{k^* c_p} + \frac{\sigma B_0^2}{\rho c_p}\right)u^{*2} - \frac{1}{\rho c_p}\frac{\partial q_r}{\partial y^*} - \frac{Q}{\rho c_p}(T^* - T^*_\infty), \tag{3}$$

$$\frac{\partial C^*}{\partial t^*} - V\frac{\partial C^*}{dy^*} = D\frac{\partial^2 C^*}{\partial y^{*2}} - K^*_C(C^* - C^*_\infty). \tag{4}$$

With boundary conditions similar to Krishna et al. [16],

$$\begin{aligned} &y^*, t^* \le 0 : v^* = 0, u^* = 0, T^* = T^*_\infty, C^* = C^*_\infty, \\ &y^* = 0, t^* > 0 : u = U_w(x) = U_0\left(1 - e^{-at}\right), T^* = T^*_w, C^* = C^*_w, \\ &y^* \longrightarrow \infty, t^* > 0 : u^* \longrightarrow 0, T^* \longrightarrow T^*_\infty, C^* \longrightarrow C^*_\infty. \end{aligned} \tag{5}$$

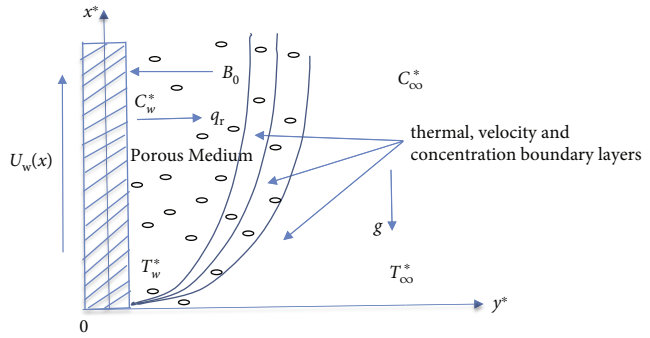

Figure 1: The fluid flow and coordinate system.

Introduce dimensionless parameters similar to Ahmed et al. [15] as follows:

$$\begin{aligned} u &= \frac{u^*}{V}, \\ y &= \frac{y^* V}{\upsilon}, \\ t &= \frac{t^* V^2}{\upsilon}, \\ M &= \frac{\sigma B_0^2 \upsilon}{\rho V^2}, \\ \mathrm{Gr} &= \frac{\upsilon g \beta_T (T^*_w - T^*_\infty)}{V^3}, \\ \mathrm{Gc} &= \frac{\upsilon g \beta_C (C^*_w - C^*_\infty)}{V^3}, \\ \mathrm{Pr} &= \frac{\upsilon}{\alpha}, \\ \theta &= \frac{T^* - T_\infty}{T^*_w - T^*_\infty}, \\ \varphi &= \frac{C^* - C^*_\infty}{C^*_w - C^*_\infty}, \\ \mathrm{Da} &= \frac{V^2 k^*}{\upsilon^2}, \\ \mathrm{Ec} &= \frac{V_2}{c_p(T^*_\infty - T^*_\infty)}, \\ \mathrm{Sc} &= \frac{\upsilon}{D}, \\ \lambda &= \frac{U_0}{V}, \\ Q &= \frac{\upsilon Q}{V^2 \rho c_p}, \\ F &= \frac{16\sigma a^* \upsilon^2 T^{*3}_\infty}{k^* U_0^2}. \end{aligned} \tag{6}$$

From Rosseland approximation,

$$\frac{\partial q_r}{\partial y^*} = -4a^*\sigma^*\left(T^{*4}_\infty - T^{*4}\right). \tag{7}$$

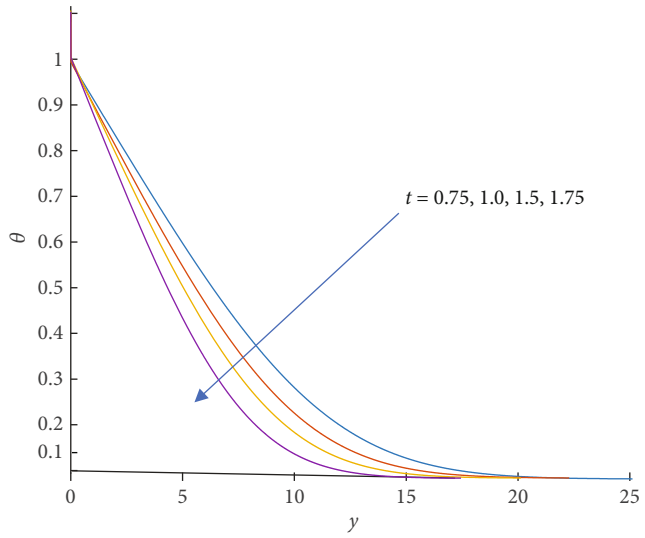

Figure 2: Different instance of time t for temperature field when Ec = 0.1, Pr = 6.2, $H = 2$, and $F = 1$.

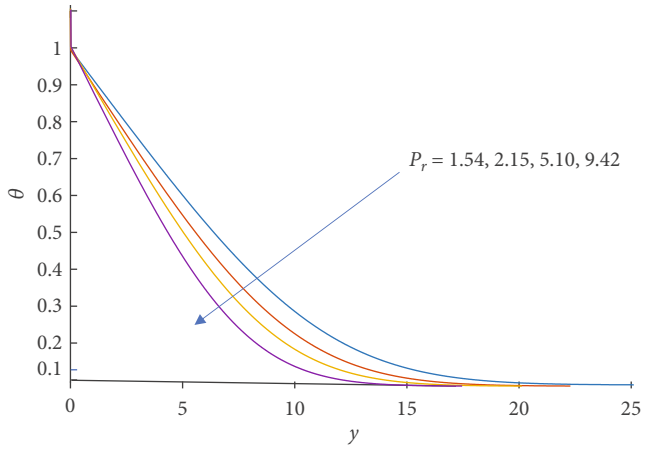

Figure 3: Distinct values of Pr for temperature field when Ec = 0.1, $t = 0.2$, $H = 2$, and $F = 1$.

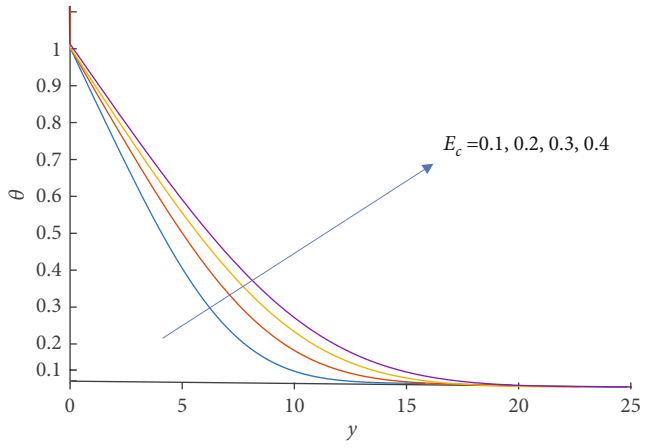

Figure 4: Distinct values of Ec for temperature field when $t = 0.2$, Pr = 6.2, $H = 2$, and $F = 1$.

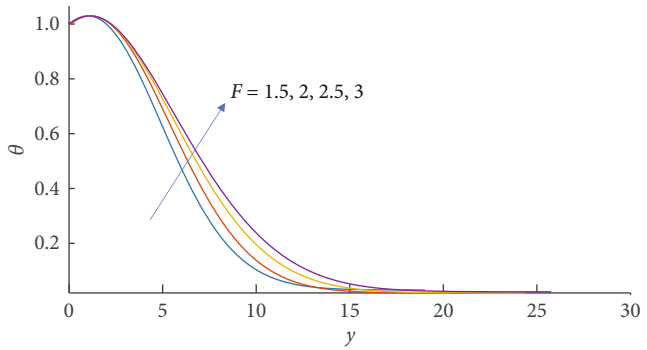

Figure 5: Increasing values of F for temperature field when $t = 0.2$, Pr = 6.2, Ec = 0.1, and $H = 2$.

Since the difference in temperature of the flow is too small and following Ahmed et al. [15] and Krishna et al. [16], expressing T^{*4} as a linear function of the temperature and applying Taylor's series expansion of T^{*4} and neglecting terms of higher order gives

$$T^{*4} \approx 4T_{\infty}^{*3}T^{*} - 3T_{\infty}^{*4}. \tag{8}$$

Substituting (8) into (7) results in

$$\frac{\partial q_r}{\partial y^{*}} = -16a^{*}\sigma T_{\infty}^{*3}(T_{\infty}^{*} - T^{*}). \tag{9}$$

With equations (6) and (9), equations (1)–(4) are transformed into the following dimensionless equations:

$$\frac{\partial u}{\partial t} - \frac{\partial u}{dy} = \frac{\partial^2 u}{\partial y^2} + G_r\theta + G_C\varphi - M_1 u. \tag{10}$$

$$\frac{\partial \theta}{\partial t} - \frac{\partial \theta}{\partial y} = \frac{1}{\mathrm{Pr}}\frac{\partial^2 \theta}{\partial y^2} + \mathrm{Ec}\left(\frac{\partial u}{\partial y}\right)^2 + \mathrm{Ec}M_1 u^2 - \frac{1}{\mathrm{Pr}}F_1\theta, \tag{11}$$

$$\frac{\partial \varphi}{\partial t} - \frac{\partial \varphi}{dy} = \frac{1}{\mathrm{Sc}}\frac{\partial^2 \varphi}{\partial y^2} - k_C\varphi, \tag{12}$$

where $F_1 = F + H$ and $M_1 = M + 1/K$.

It is associated with dimensionless boundary conditions as follows:

$$\theta = 0, \varnothing = 0, u = 0, \text{for } t \le 0, \tag{13}$$

$$\theta = 1, \varnothing = 1, u = \lambda\left(1 - e^{-mt}\right), \text{for } y = 0, t > 0, \tag{14}$$

$$\theta \longrightarrow 0, \varnothing \longrightarrow 0, u \longrightarrow 0 \text{ as } y \longrightarrow \infty, t > 0. \tag{15}$$

3. Approximate Analytic Method

The nonlinearly transformed dimensionless equations (10)–(12) subject to boundary conditions in (13) are solved using approximate analytic method outlined below. This method is similar to numerical/Laplace transform solution proposed by Ahmed et al. [15] but novel. Generally, these nonlinear equations must be integrated numerically, but for a case where the Reynolds number is small, approximate

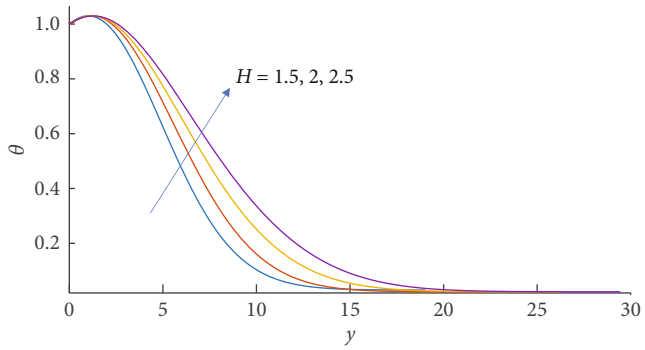

FIGURE 6: Increasing values of H for temperature field when $t = 0.2$, Pr = 6.2, Ec = 0.1, and $F = 1$.

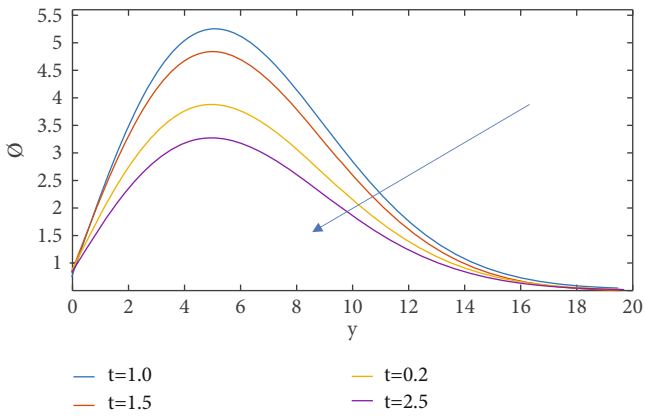

FIGURE 7: Distinct values of time t for concentration field when Kc = 1.5, Ec = 0.1, and Sc = 2.01.

analytic solution can be found by applying perturbation method. By using this technique, a linear approximated solution of the nonlinear equations is found.

Now considering the dimensionless concentration model in (12), expanding in terms of Eckert number using power series gives

$$\sum_{i=1}^{n} \varnothing_n'(t)E_c^n(y) - \sum_{i=1}^{n} \varnothing_n(t)\frac{\partial}{\partial y}(E_c^n(y)) = \frac{1}{S_c}\left[\sum_{i=1}^{n} \varnothing_n(t)\frac{\partial^2}{\partial y^2}(E_c^n(y))\right] - k_c\left[\sum_{i=1}^{n} \varnothing_n'(t)E_c^n(y)\right],$$

$$\begin{aligned}&\left[\varnothing_0' + \varnothing_1'E_c + \varnothing_2'E_c^2\right] - \left[\varnothing_1 + 2\varnothing_2E_c + 3\varnothing_3E_c^2\right]\frac{\partial E_c}{\partial y} = \frac{1}{S_c}\left[2\varnothing_2 + 6\varnothing_3E_c + 12\varnothing_4E_c^2\right]\left(\frac{\partial E_c}{\partial y}\right)^2 \\ &+ \frac{1}{S_c}\left[\varnothing_1 + 2\varnothing_2E_c + 3\varnothing_3E_c^2\right]\frac{\partial^2 E_c}{\partial y^2} - k_c\left[\varnothing_0 + \varnothing_1E_c + \varnothing_2E_c^2\right].\end{aligned} \tag{16}$$

Considering powers of Ec,

$$E_c^0 : \varnothing_0' - \varnothing_1\frac{\partial E_c}{\partial y} = \frac{2\varnothing_2}{S_c}\left(\frac{\partial E_c}{\partial y}\right)^2 + \frac{\varnothing_1}{S_c}\frac{\partial^2 E_c}{\partial y^2} - k_c\varnothing_0, \tag{17}$$

$$E_c^1 : \varnothing_1' - 2\varnothing_2\frac{\partial E_c}{\partial y} = \frac{6\varnothing_3}{S_c}\left(\frac{\partial}{\partial y}\right)^2 + \frac{2\varnothing_2}{S_c}\frac{\partial^2}{\partial y^2} - k_c\varnothing_1, \tag{18}$$

$$E_c^2 : \varnothing_2' - 3\varnothing_3\frac{\partial E_c}{\partial y} = \frac{12\varnothing_4}{S_c}\left(\frac{\partial E_c}{\partial y}\right)^2 + \frac{3\varnothing_3}{S_c}\frac{\partial^2 E_c}{\partial y^2} - k_c\varnothing_2. \tag{19}$$

In power series, the coefficient terms are such that $\varnothing_0 > \varnothing_1 > \varnothing_2 \cdots$; hence, higher terms will be neglected. Also, the Eckert numbers are chosen to be less than 1 (i.e., $E_c < 1$); hence, terms such us E_c^2, E_c^3, E_c^4, will be much smaller hence neglected.

In (19),

$$\frac{d\varnothing_2}{dt} + k_c\varnothing_2 = 0, \tag{20}$$

$$\varnothing_2(t) = ce^{-k_ct}. \tag{21}$$

From boundary conditions in (13), $\varnothing = 1$ for all $y = 0$, $t \geq 0$ put in (20) gives

$$\varnothing_2(t) = e^{-k_ct}. \tag{22}$$

Applying Laplace transform to (18) gives

$$s\overline{\varnothing}_1(y,s) - \varnothing(y,0) - \frac{2}{k_c+s}\frac{\partial \bar{E}_c}{\partial y} - \frac{2}{S_c}\frac{1}{k_c+s}\frac{\partial^2 \bar{E}_c}{\partial y^2} + k_c\overline{\varnothing}_1(y,s) = 0. \tag{23}$$

But $\varnothing(y,0) = 0$

$$\frac{2}{S_c}\frac{1}{k_c+s}\frac{\partial^2 \bar{E}_c}{\partial y^2} + \frac{2}{k_c+s}\frac{\partial \bar{E}_c}{\partial y} = \overline{\varnothing}_1(s+k_c). \tag{24}$$

Equation (24) is linear nonhomogeneous second-order ODE.

The general solution (24) is

$$\bar{E}_c = \bar{E}_ce^{-S_cy} + \frac{1}{2}\overline{\varnothing}_1(s+k_c)^2, \tag{25}$$

$$\overline{\varnothing}_1 = \frac{2\bar{E}_c}{(s+k_c)^2} - \frac{2\bar{E}_ce^{-S_cy}}{(s+k_c)^2}. \tag{26}$$

By convolution theorem, in (26), the inverse Laplace transform is

$$\varnothing_1 = 2E_ce^{-k_ct}t - 2E_ce^{-k_ct-S_cy}t. \tag{27}$$

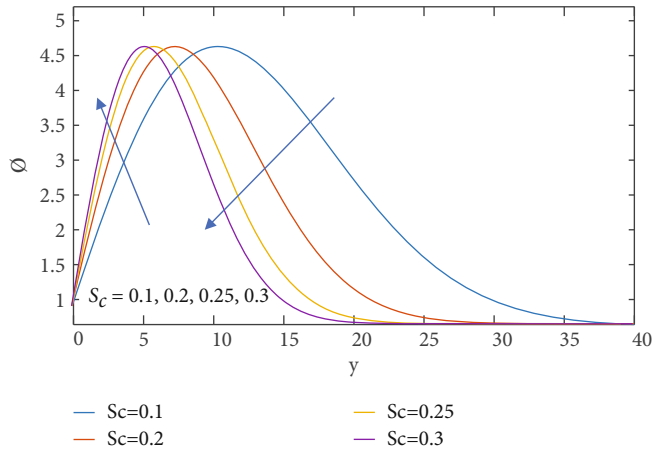

Figure 8: Distinct values of Sc for concentration field when Ec = 0.1, $t = 0.2$, and Kc = 1.

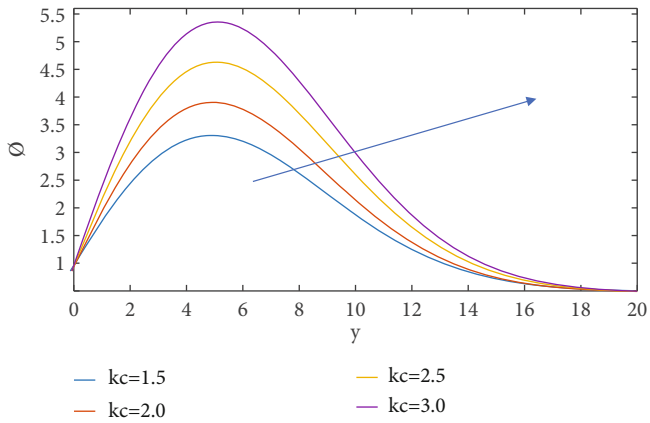

Figure 9: Distinct values of Kc for concentration field when Ec = 0.1, $t = 0.2$, and Sc = 2.01.

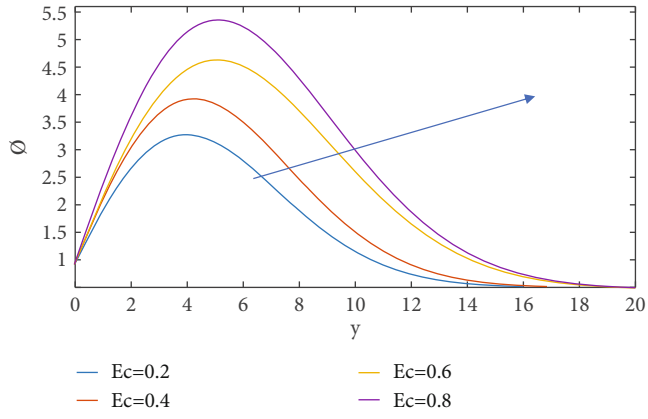

Figure 10: Distinct values of Ec for concentration field when $t = 0.2$, Kc = 1, and Sc = 2.01.

Similarly, the Laplace transform of (17) gives

$$\frac{1}{S_c}\left[\frac{2\bar{E}_c}{(s+k_c)^2}-\frac{2\bar{E}_c e^{-S_c y}}{(s+k_c)^2}\right]\frac{\partial^2\bar{E}_c}{\partial y^2}+\left[\frac{2\bar{E}_c}{(s+k_c)^2}-\frac{2\bar{E}_c e^{-S_c y}}{(s+k_c)^2}\right]\frac{\partial\bar{E}_c}{\partial y}=\overline{\varnothing}_0(s+k_c). \tag{28}$$

The general solution of (28) is

$$\bar{E}_c=\bar{E}_c e^{-S_c y}+\frac{\overline{\varnothing}_0(s+k_c)(s+k_c)^2 1}{2\bar{E}_c-2\bar{E}_c e^{-S_c y}}, \tag{29}$$

$$\overline{\varnothing}_0=\frac{\bar{E}_c\left(2\bar{E}_c-2\bar{E}_c e^{-S_c y}\right)}{(s+k_c)(s+k_c)^2}-\frac{\bar{E}_c e^{-S_c y}\left(2\bar{E}_c-2\bar{E}_c e^{-S_c y}\right)}{(s+k_c)(s+k_c)^2}. \tag{30}$$

Applying convolution theorem in (30) gives the inverse Laplace transform as

$$\varnothing_0=\frac{t^2E_c}{2}e^{-k_c t}\left(2E_c-2E_c e^{-S_c y}\right)-\frac{t^2E_c}{2}e^{S_c y-k_c t}\left(2E_c-2E_c e^{-S_c y}\right). \tag{31}$$

The general solution of the concentration model is

$$\varnothing(y,t)=\varnothing_o+\varnothing_1E_c+\varnothing_2E_c^2+\cdots,$$

$$\varnothing(y,t)=\frac{t^2E_c}{2}e^{-k_c t}\left(2E_c-2E_c e^{-S_c y}\right)\left(1-e^{-S_c y}\right)+2tE_c e^{-k_c t}\left(1-e^{-S_c y}\right)E_c+e^{-k_c t}E_c^2. \tag{32}$$

Similarly, by considering the dimensionless temperature model in (11) and the dimensionless velocity model in (10), expanding in power series in terms of Eckert number, the

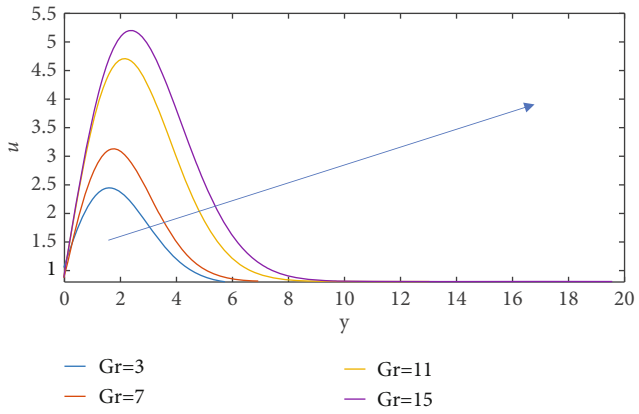

Figure 11: Increasing values of Gr for velocity field when $\lambda = 1$, $M = 2$, Kc = 1.5, $k = 1$, $F = 1$, Gc = 5, Sc = 2.01, Pr = 6.2, Ec = 0.1, $m = 1$, $H = 2$, and $t = 1$.

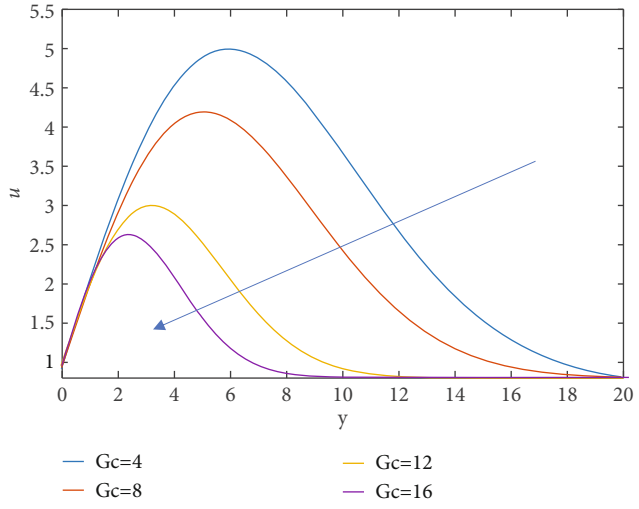

Figure 12: Distinct values of Gc for velocity field when $M = 2$, $t = 2$, Kc = 1.5, $k = 1$, Gr = 5, Ec = 0.1, $F = 1$, Sc = 2.01, $m = 1$, $H = 2$, $\lambda = 1$, and Pr = 6.2.

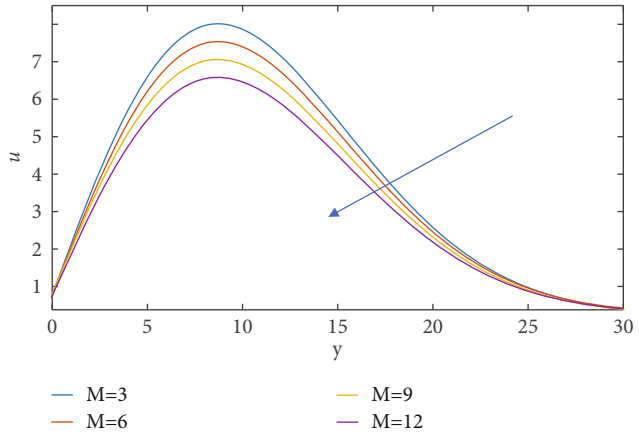

Figure 13: Increasing values of M for velocity field when Gr = 5, $t = 2$, Kc = 1.5, $k = 1$, Gc = 5, Ec = 0.1, Pr = 6.2, $m = 1$, Sc = 2.01, $\lambda = 1$, $H = 2$, and $F = 1$.

general solutions are, respectively,

$$\theta(y,t) = \frac{t^2 E_c}{2} e^{-F_1/P_r t}\left(2E_c - 2E_c e^{-P_r y}\right)\left(1 - e^{-P_r y}\right) + 2tE_c e^{-F_1/P_r t}\left(1 - e^{-P_r y}\right)E_c + e^{-F_1/P_r t}E_c^2,$$

$$u(y,t) = \left[2\lambda E_c e^{-M_1 t}\left(t + \frac{e^{-mt}}{m}\right)\left(1 - e^{-y}\right) + \frac{1}{m}2\lambda E_c e^{-M_1 t}\left(e^{-y} - 1\right) + G_r\theta_1 e^{-M_1 t} + G_c\varnothing_1 e^{-M_1 t}\right]\left[E_c e^{-M_1 t} - E_c e^{-y - M_1 t} + E_c\right] + G_r\theta_0 e^{-M_1 t} + G_c\varnothing_0 e^{-M_1 t} + \lambda\left(1 - e^{-mt}\right)e^{-M_1 t}E_c^2, \tag{33}$$

where $\theta_0 = \left(2E_c - 2E_c e^{-P_r y}\right)\left(t^2 E_c/2e^{-F_1/P_r t} - t^2 E_c/2\right.$ $\left.e^{-P_r y - F_1/P_r t}\right)$

$$\theta_1 = 2E_c te^{-F_1/P_r t} - 2E_c te^{-F_1/P_r t - P_r y},$$

$$\varnothing_0 = \left(2E_c - 2E_c e^{-S_c y}\right)\left(\frac{t^2 E_c}{2}e^{-k_c t} - \frac{t^2 E_c}{2}e^{-S_c y - k_c t}\right), \tag{34}$$

$$\varnothing_1 = 2E_c te^{-k_c t} - 2E_c te^{-k_c t - S_c y}.$$

After obtaining the temperature field, it is possible to investigate the heat transfer coefficient rate at the stretched plate in terms of the Nu. The t, F, H, Ec, and Pr effects on Nu can be investigated. The dimensionless Nusselt number is

$$\mathrm{Nu} = -\left.\frac{\partial\theta}{\partial y}\right|_{y=0} = 2P_r tE_c^2 e^{-F_1/P_r t}. \tag{35}$$

The mass transfer coefficient rate at the stretching plate in terms of the Sh can be calculated from the concentration field. The t, Ec, Sc, and Kc effects on Sherwood number are investigated. The Sherwood number is

$$\mathrm{Sh} = -\left.\frac{\partial\varnothing}{\partial y}\right|_{y=0} = 2S_c tE_c^2 e^{-k_c t}. \tag{36}$$

After obtaining the velocity profile, it is also important to investigate variations in skin friction as a result of the physical parameters t, m, M, H, Ec, Pr, Kc, k, Gr, and Gc. The skin friction is

$$\tau = \left.\frac{\partial u}{\partial y}\right|_{y=0} = 2\lambda E_c^2 e^{-M_1 t}\left(t + \frac{e^{-mt}}{m}\right) - \frac{2}{m}\lambda E_c^2 e^{-M_1 t} + 2P_r G_r E_c^2 te^{-F_1/P_r - M_1 t} + 2\lambda S_c G_c E_c^2 te^{-k_c t - M_1 t}. \tag{37}$$

4. Results and Discussion

The physical dynamics of the problem can be studied, the controlling parameters effects on the temperature (θ),

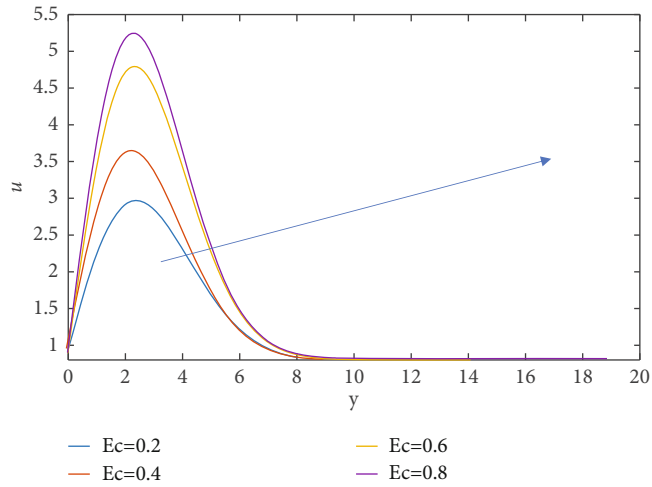

Figure 14: Increasing values of Ec for velocity field when Gr = 5, $t = 2$, Kc = 1.5, $k = 1$, Gc = 5, $M = 5$, Pr = 6.2, $m = 1$, Sc = 2.01, $\lambda = 1$, $H = 2$, and $F = 1$.

Table 1: Distinct values of t, F, Ec, H, and Pr for the Nusselt number $(-\varnothing'(0))$ at the wall.

t	H	Ec	Pr	F	$-\varnothing'(0)$
0.2	1.0	0.9	1.0	1.0	0.2172
0.4	1.0	0.9	1.0	1.0	0.2912
0.2	0.2	0.9	1.0	1.0	0.2549
0.2	0.4	0.9	1.0	1.0	0.2449
0.2	1.0	0.7	1.0	1.0	0.1314
0.2	1.0	0.9	1.0	1.0	0.2172
0.2	1.0	0.9	3.1	1.0	0.3120
0.2	1.0	0.9	6.2	1.0	0.5172
0.2	1.0	0.9	1.0	0.2	0.2549
0.2	1.0	0.9	1.0	0.4	0.2449

Table 2: Distinct values of t, Sc, Kc, and Ec for Sherwood number $(-\varnothing'(0))$ at the wall.

t	Sc	Kc	Ec	$-\varnothing'(0)$
0.2	1.0	0.5	0.9	0.2932
0.4	1.0	0.5	0.9	0.5305
0.2	0.7	0.5	0.9	0.2052
0.2	0.9	0.5	0.9	0.2639
0.2	1.0	0.4	0.9	0.2991
0.2	1.0	0.6	0.9	0.2874
0.2	1.0	0.5	0.7	0.1773
0.2	1.0	0.5	0.9	0.2932

velocity (u), and concentration ($\varnothing$) profiles are illustrated graphically using a written MATLAB codes. Numerically, the values of local Nusselt number $(-\theta'(0))$, skin friction coefficient $(-u'(0))$, and Sherwood number $(-\varnothing'(0))$ are presented in tables.

4.1. Graphical Results

4.1.1. Temperature Profiles. Figure 2 illustrates the temperature profiles indicating the effects of time, t. The fluid temperature decreases as time passes. Figures 3 and 4 show the effects of Prandtl number (Pr) and Eckert number (Ec) on the temperature profiles, respectively. Increase in Pr decreases the thermal boundary layer thickness of the fluid whilst increase in Ec increases the fluid temperature. Physically, increasing Pr results in decreasing the thermal conductivity of fluid and increase in viscosity of fluid; hence, the thermal boundary layer decreases. Since Ec relates the kinetic energy in the flow and the heat enthalpy, so the kinetic energy of the fluid is amplified by increasing Ec; hence, the temperature of the fluid increases.

Figures 5 and 6 show the temperature profile of the effects of radiation parameter (F) and heat absorption parameter (H), respectively. From the graphs, temperature increases with increase in either F or H. Physically, the radiation parameter relates the conduction heat transfer to the thermal radiation transfer. So an increased in the radiation parameter caused the temperature within the boundary layer to rise.

4.1.2. Concentration Profiles. In Figures 7–10, illustrate the concentration profiles of the effects of t, Sc, Kc, and Ec, respectively. It is noticed that there is a decrease in the concentration of the fluid as time passes resulting in decrease in porous medium permeability. Initially, increase in Sc increases the concentration boundary layer thickness but at the twist of the flow, further increase in Sc decreases concentration as a result of the unsteadiness in the flow. This is also due to the fact that, physically, the molecular diffusivity of a fluid decreases as Sc increases causing a reduction in the concentration boundary layer thickness. However, the concentration of the fluid increases as Kc or Ec increases due to enhancement of the kinetic energy of the fluid. The fluid converged at termination point for concentration field for Kc and Ec, as shown in the diagrams.

Table 3: Distinct values of H, t, Ec, M, Pr, Sc, F, Gr, Kc, Gc, k when $\lambda = 1$, and $m = 1$ for the skin friction coefficient $(-u'(0))$.

t	M	F	Ec	Pr	Gr	Gc	Sc	Kc	k	H	$-u'(0)$
0.4	1.2	1.5	0.7	1.2	1.5	1.5	1.2	1.3	1.3	1.5	1.6762
0.7	1.2	1.5	0.7	1.2	1.5	1.5	1.2	1.3	1.3	1.5	1.6142
0.3	1.4	1.5	0.7	1.2	1.5	1.5	1.2	1.3	1.3	1.5	1.6511
0.3	2.2	1.5	0.7	1.2	1.5	1.5	1.2	1.3	1.3	1.5	1.6158
0.3	1.2	2.5	0.7	1.2	1.5	1.5	1.2	1.3	1.3	1.5	1.3125
0.3	1.2	3.0	0.7	1.2	1.5	1.5	1.2	1.3	1.3	1.5	1.3543
0.3	1.2	1.5	0.8	1.2	1.5	1.5	1.2	1.3	1.3	1.5	1.6451
0.3	1.2	1.5	0.9	1.2	1.5	1.5	1.2	1.3	1.3	1.5	1.6252
0.3	1.2	1.5	0.7	2.8	1.5	1.5	1.2	1.3	1.3	1.5	1.7823
0.3	1.2	1.5	0.7	6.2	1.5	1.5	1.2	1.3	1.3	1.5	1.8945
0.3	1.2	1.5	0.7	1.2	2.0	1.5	1.2	1.3	1.3	1.5	1.8188
0.3	1.2	1.5	0.7	1.2	2.5	1.5	1.2	1.3	1.3	1.5	1.7934
0.3	1.2	1.5	0.7	1.2	1.5	2.0	1.2	1.3	1.3	1.5	1.7716
0.3	1.2	1.5	0.7	1.2	1.5	2.5	1.2	1.3	1.3	1.5	1.7402
0.3	1.2	1.5	0.7	1.2	1.5	1.5	2.0	1.3	1.3	1.5	1.7172
0.3	1.2	1.5	0.7	1.2	1.5	1.5	2.5	1.3	1.3	1.5	1.8223
0.3	1.2	1.5	0.7	1.2	1.5	1.5	1.2	0.1	1.3	1.5	1.3922
0.3	1.2	1.5	0.7	1.2	1.5	1.5	1.2	0.2	1.3	1.5	1.3215
0.3	1.2	1.5	0.7	1.2	1.5	1.5	1.2	1.3	0.2	1.5	14812
0.3	1.2	1.5	0.7	1.2	1.5	1.5	1.2	1.3	0.4	1.5	14661
0.3	1.2	1.5	0.7	1.2	1.5	1.5	1.2	1.3	1.3	2.5	1.3125
0.3	1.2	1.5	0.7	1.2	1.5	1.5	1.2	1.3	1.3	3.0	1.3543

Table 4: Comparison of results of temperature, $t = 1$, Ec = 0.3, $F = 0.5$, $H = 1$, and $y = 2$.

Pr	Ahmed et al. [15] (Crank-Nicolson method)	Krishna et al. [16] (Laplace transform techniques)	Present study (approximate analytic method)
0.71	0.0711189	0.0711681	0.071153
3	0.0025077	0.0025271	0.0026165
7	0.0000181	0.0000186	0.0000183

Table 5: Comparison of results of velocity, $M = 0.5$, Sc = 0.22, $k = 0.5$, Pr = 0.71, $F = 1$, Gr = 5, $t = 1$, Ec = 0.3, $F = 0.5$, $H = 1$, $m = 1$, $\lambda = 0.5$, $\omega = 0$, and $y = 2$.

Gc	Ahmed et al. [15] (Crank-Nicolson method)	Krishna et al. [16] (Laplace transform techniques)	Present study (approximate analytic method)
5	0.384885	0.384775	0.384863
7	0.432656	0.432589	0.432742
10	0.548079	0.547087	0.548157
12	0.632847	0.632256	0.632646

4.1.3. Velocity Profiles. Figures 11–14 show the profiles of the velocity of the effects of thermal Grashof number (Gr), mass Grashof number (Gc), magnetic parameter (M), and Eckert number (Ec), respectively. In Figure 11, increase in Gr increases the speed of the flow as a result of the strength in the buoyancy force aiding the velocity to raise in the boundary layer. In Figure 12, however, increase in Gc decreases the velocity due to the delay in convection motion of the fluid as a result of the magnetic field influence. Also, in Figure 13, the fluid velocity diminishes as M increases. In practice, this is true because magnetic field produces a Lorentz force that has the tendency to retard a free convective flow. The kinetic energy of the fluid is amplified due to increase in Eckert number (Ec) resulting in increase of the velocity of the fluid as depicted in Figure 14.

Table 6: Comparison of results of concentration, Kc = 0.5, Ec = 0.3 , $t = 1$, and $y = 2$.

Sc	Ahmed el al. [15] (Crank-Nicolson method)	Krisna et al. [16] (Laplace transform techniques)	Present study (approximate analytic method)
0.22	0.284308	0.284447	0.283317
0.3	0.228051	0.228774	0.227642
0.6	0.167541	0.164551	0.167632
0.78	0.084308	0.081447	0.083421

4.2. Numerical Results. Tables 1–3 illustrate the behaviour of Nusselt number, $-\theta'(0)$, Sherwood number, $-\varnothing'(0)$, and skin friction coefficient, $-u'(0)$ for distinct values of t, M, Ec, Kc, Pr, Sc, k, H, Gr, F, and Gc. In Table 1, Nusselt number, $-\theta'(0)$ rises with increase in t, Ec, and Pr; it however decreases as H and F increase. Table 2 shows that the Sherwood number, $-\varnothing'(0)$, decreases as Kc increases but increases for increase in t, Sc, and Ec. In Table 3, it is noticed that skin friction coefficient diminishes for increase in t, M, Ec, k, Kc, Gr, and Gc but increases for increasing values of Pr, F, Sc, and H. The controlling parameters such as t, M, Ec, k, Kc, Gr, and Gc are effective in reducing skin friction in chemically reactive magnetic porous medium and are relevant in practice. This is good in practice because reduced skin friction enhances the efficiency of a system. For example, fuel efficiency of many equipment is improved due to reduced skin friction. In Tables 4–6, present study results are compared with previous results of Ahmed et al. [15] and Krishna et al. [16] and there is consistency.

5. Conclusion

A magnetohydrodynamic fluid flow across a stretching vertical plate in a chemically unsteady porous reactive medium has been studied. Dimensionless parameters are used to model the associated partial differential equations into dimensionless differential equations. Approximate analytic method was employed to solve the resulting dimensionless equations, and the results obtained are shown in graphs and tables. From the graphical and numerical results obtained, it was established that

(1) The thermal boundary layer thickness decreases with Prandtl number as time passes but increases with the

radiation parameter, Eckert number, and the heat absorption parameter

(2) The concentration boundary layer thickness diminishes with time but increases with the rate of chemical reaction in the fluid, Eckert number, and Schmidt number. It is however noticed that there is a reduction in the species concentration in the fluid due to the Schmidt number at the twist of the flow

(3) The velocity diminishes with increase in the mass Grashof number and magnetic parameter but increases with increase in thermal Grashof number and Eckert number

(4) As time passed, reduced skin friction is achieved with increase in either the permeability of porous medium, chemical reaction parameter, Eckert number, thermal Grashof number, or the mass Grashof number

In general, the results obtained in the current study indicate that chemically reactive magnetic field can be used to influence a flow field. The controlling parameters such as t, M, Ec, k, Kc, Gr, and Gc are effective in reducing skin friction in chemically reactive magnetic porous medium and are relevant in practice because reduced skin friction enhances the efficiency of a system. For example, fuel efficiency of many equipment is improved due to reduced skin friction. The results of the current study are useful in solar energy collector systems and material processing.

Nomenclature

u^*,v^*: x and y components of velocity, respectively (ms^{-1})
U_0: Velocity of the plate (ms^{-1})
y^*: Coordinate axis normal to the plate (m)
t^*: Time (s)
v: Kinematic viscosity ($m^2\,s^{-1}$)
β_T: Thermal expansion coefficient (K^{-1})
β_C: Concentration expansion coefficient (K^{-1})
ρ: Fluid density (kgm^{-3})
T^*: Fluid temperature near the plate (K)
T_w^*: Fluid temperature at the plate surface (K)
T_∞^*: Temperature of the free stream (K)
C^*: Concentration in the fluid ($Kmolm^{-3}$)
C_∞^*: Concentration far away from the plate ($Kmolm^{-3}$)
C_w^*: Concentration at the plate surface ($Kmolm^{-3}$)
a: Acceleration parameter (-)
D: Chemical molecular diffusivity ($m^{-2}\,s^{-1}$)
$\propto$: Thermal diffusivity ($m^2\,K^{-1}$)
C_p: Specific heat at constant pressure ($Jkg^{-1}\,K^{-1}$)
K_c^*: Rate of chemical reaction (-)
k^*: Permeability coefficient of the porous medium (m^2)
q_r: Radiation heat flux (-)
Q: Heat source parameter (-)
y: Dimensionless coordinate axis normal to the plate surface (-)
u: Dimensionless velocity in x direction (-)
v: Dimensionless velocity in y direction (-)
θ: Dimensionless temperature (-)
t: Dimensionless time (-)
k: Dimensionless permeability of the porous medium (-)
F: Radiation parameter (-)
M: Magnetic parameter (-)
H: Heat absorption parameter (-)
A: Constant (-)
B_0: Uniform external magnetic field (Telsa)
μ: Dynamic viscosity ($kgm^{-1}\,s^{-1}$)
S_0: Soret number (-)
Sc: Schmidt number (-)
Pr: Prandtl number (-)
Gr: Thermal Grashof number (-)
Gc: Mass Grashof number (-)
σ: Electrical conductivity (sm^{-1})
$\varnothing$: Dimensionless concentration in the fluid (-)
g: Acceleration due to gravity (ms^{-2})
K: Thermal conductivity of the fluid ($Wm^{-1}\,K^{-1}$)
Kc: Dimensionless rate of chemical reaction (-)
Ec: Eckert number (-)
a^*: Rosseland mean absorption coefficient (-)
σ^*: Stefan-Boltzman constant (-).

Data Availability

Numerical data used to support the findings of this study are included within the article.

Conflicts of Interest

The authors declare that they have no conflicts of interest.

References

[1] H. S. Carslaw and J. C. Jaeger, *Conduction of Heat in Solids*, Oxford University Press, Landon, 1959.

[2] B. C. Sakiadis, "Boundary layer behaviour on continuous solid surfaces," *AIChE Journal*, vol. 7, no. 1, pp. 26–28, 1961.

[3] L. J. Crane, ""Flow past a stretching plate", Journal of Applied," *Zeitschrift für angewandte Mathematik und Physik ZAMP*, vol. 21, no. 4, pp. 645–647, 1970.

[4] T. C. Chiam, "Heat transfer in a fluid with variable thermal conductivity over a linearly stretching sheet," *Acta Mechanica*, vol. 129, no. 1-2, pp. 63–72, 1998.

[5] M. Misra, N. Ahmad, and Z. U. Siddiqui, "Unsteady boundary layer flow past a stretching plate and heat transfer with variable thermal conductivity," *World Journal of Mechanics*, vol. 2, no. 1, pp. 35–41, 2012.

[6] C. H. Chen, "Laminar mixed convection adjacent to vertical continuously stretching sheets," *Heat and Mass Transfer*, vol. 33, no. 5-6, pp. 471–476, 1998.

[7] A. Ishak, R. Nazar, and I. Pop, "Hydromagnetic flow and heat transfer adjacent to a stretching vertical sheet," *Heat and Mass Transfer*, vol. 44, no. 8, pp. 921–927, 2008.

[8] B. S. Dandpat and S. Chakraborthy, "Effects of variable fluid properties on unsteady thin film flow over a non-linear stretching sheet," *International Journal of Heat and Mass Transfer*, vol. 53, no. 25-26, pp. 5757–5763, 2010.

[9] K. L. Hsiao, "Heat and mass mixed convection for MHD viscoelastic fluid past a stretching sheet with Ohmic dissipation," *Communications in Nonlinear Science and Numerical Simulation*, vol. 15, no. 7, pp. 1803–1812, 2010.

[10] K. L. Hsiao, "MHD stagnation point viscoelastic fluid flow and heat transfer on a thermal forming stretching sheet with viscous dissipation," *The Canadian Journal of Chemical Engineering*, vol. 89, no. 5, pp. 1228–1235, 2011.

[11] S. Nadeem, R. U. Haq, N. S. Akbar, and Z. H. Khan, ""MHD three-dimensional Casson fluid flow past a porous linearly stretching sheet", Alexendra," *Alexandria Engineering Journal*, vol. 52, no. 4, pp. 577–582, 2013.

[12] Y. I. Seini and O. D. Makinde, "MHD boundary layer flow due to exponential stretching surface with radiation and chemical reaction," *Mathematical Problems in Engineering*, vol. 2013, 7 pages, 2013.

[13] M. Ali, M. D. Abdul-Alim, and M. S. Alam, "Heat transfer boundary layer flow past an inclined stretching sheet in the presence of magnetic field," *International Journal of Advanced Research and Technology*, vol. 3, no. 5, pp. 34–40, 2014.

[14] A. C. Sahoo and T. Biswal, "MHD viscoelastic boundary layer flow past a stretching plate with heat transfer," *IJETMAS*, vol. 3, no. 9, pp. 11–18, 2015.

[15] S. Ahmed, A. Batin, and A. J. Chamkha, "Numerical/Laplace transform analysis for MHD radiating heat/mass transport in a Darcian porous regime bounded by an oscillating vertical surface," *Alexandria Engineering Journal*, vol. 54, no. 1, pp. 45–54, 2015.

[16] M. Veera Krishna, M. Gangadhar Reddy, and J. A. Chamkha, "Heat and mass transfer on unsteady MHD flow through an infinite oscillating vertical porous surface," *Journal of Porous Media*, vol. 24, no. 1, pp. 81–100, 2021.

[17] M. Sulemana, I. Y. Seini, and M. I. Daabo, "Unsteady boundary layer flow past a vertical plate in the presence of transverse magnetic field and heat source embedded in a porous medium," *Journal of Mathematical and Computational Science*, vol. 7, no. 3, pp. 564–582, 2017.

[18] M. Sulemana, I. Y. Seini, and M. I. Daabo, "Unsteady hydromagnetic convective heat and mass transfer flow past an impulsively started infinite vertical surface with Newtonian heating in a porous medium," *Journal of Engineering and Applied Sciences*, vol. 12, no. 1, pp. 5767–5776, 2017.

[19] M. Sulemana and I. Y. Seini, "Time-dependent hydromagnetic boundary layer flow across a porous vertical surface with internal heat generation," *Defect and Diffusion Forum*, vol. 409, pp. 17–38, 2021.

[20] A. Hussain, M. Y. Malik, M. Khan, and T. Salahuddin, "Application of generalized Fourier heat conduction law on MHD viscoinelastic fluid flow over stretching surface," *International Journal of Numerical Methods for Heat & Fluid Flow*, vol. 30, no. 6, pp. 3481–3496, 2020.

[21] S. Khan, M. M. Selim, A. Khan et al., "On the analysis of the non-Newtonian fluid flow past a stretching/shrinking permeable surface with heat and mass transfer," *Coatings*, vol. 11, no. 5, p. 566, 2021.

[22] N. S. Yousef, A. M. Megahed, N. I. Ghoneim, M. Elsafi, and E. Fares, "Chemical reaction impact on MHD dissipative Casson-Williamson nanofluid flow over a slippering stretching sheet through porous medium," *Alexandria Engineering Journal*, vol. 61, no. 12, pp. 10161–10170, 2022.

[23] A. Saeed, E. A. Algehyne, M. S. Aldhabani, A. Dawar, P. Kumam, and W. Kunam, "Mixed convective flow of a magnetohydrodynamic Casson fluid through a permeable stretching sheet with first-order chemical reaction," *PLoS One*, vol. 17, no. 4, article e0265238, 2022.

[24] E. A. Algehyne, M. Areshi, A. Saeed, A. Dawar, Z. Shah, and P. Kumam, "Three-dimensional MHD flow of Casson fluid past an exponentially stretching/shrinking sheet with homogeneous-heterogeneous reactions," *Waves in Random and Complex Media*, vol. 32, pp. 1–22, 2022.

[25] H. U. Rasheed, S. Islam, Z. Shan et al., "Numerical modeling of unsteady MHD flow of Casson fluid in a vertical surface with chemical reaction and hall current," *Advances in Mechanical Engineering*, vol. 14, no. 3, Article ID 16878132221085429, 2022.